Chromophore Orientations in a Nonlinear Optical Azopolymer Diffraction Grating: Even and Odd Order Parameters from Far-Field Raman and Near-Field Second Harmonic Generation Microscopies

F. Lagugné-Labarthet* and C. Sourisseau

LPCM, UMR 5803 CNRS, Université Bordeaux 1, 351 Cours de la Libération, 33405 Talence Cedex, France

R. D. Schaller and R. J. Saykally

Department of Chemistry, University of California, Berkeley, California, 94720-1460

P. Rochon

Department of Physics, Royal Military College, Kingston, Ontario, Canada, K7K 5L0

Received: July 1, 2004; In Final Form: August 19, 2004

A diffraction grating with a large diffraction efficiency ($\eta = 25\%$ on the first order) was inscribed on an azobenzene-containing polymer thin film, electrically poled, and characterized using spatially resolved Raman confocal microscopy and near-field scanning optical microscopy (NSOM) coupled with second-order nonlinear optical measurements. Linear (Raman) and nonlinear (second harmonic generation or SHG) polarized microscopic measurements were performed on a grating with ~1.4 μm periodicity, revealing the molecular orientations in various regions of the sinusoidal relief surface. The most probable distribution functions $f(\theta)$ of the chromophore orientations were derived using the two first even parity Legendre polynomials $\langle P_2 \rangle$ and $\langle P_4 \rangle$ together with the two odd order parameters $\langle P_1 \rangle$ and $\langle P_3 \rangle$, as determined by Raman and SHG, respectively. These distribution functions show that the poling treatment is quite efficient and also emphasize the importance of determining both couples of the order parameters in such a surface-modulated optical element. In particular, new information is provided about the formation mechanism of the additional surface modulations of half periodicity that are revealed by the SHG-NSOM data but are not detected in the far-field Raman scattering measurements.

I. Introduction

Mesostructured materials with large optical nonlinearities have many potential applications in the field of telecommunication as splitters, waveguides, high-speed light modulators and resonators, wavelength converters, and polarization discriminators.[1−4] More specifically, $\chi^{(2)}$ gratings inscribed on polymer thin films are important and attractive components allowing the generation and separation of the second harmonic wave from the fundamental input wave; they represent excellent alternatives to inorganic materials in terms of processability, reliability and low cost. As an example, such devices are key elements for integrated optics in distributed feedback lasers,[5−8] in which the laser emission at the second harmonic wavelength arises from the noncentrosymmetrically organized material and the oscillation is ensured by a diffraction grating instead of a cavity.

To fabricate periodic nonlinear optical structures, many authors have made use of various possibilities, such as embossing together with poling,[9] photoalignment through a mask,[2] all-optical poling methods,[4,10,11] and direct corona electrical poling conditions. The poling process conducted during [12] or after [8,13] inscription of the surface relief gratings on azobenzene-functionalized polymer thin films was also another very efficient and practical method. In the present study, a surface relief grating was first fabricated in one step by holography on a thin film of p(DR1M), [poly(4′(((2-(methacryloyloxy)ethyl)ethyl)-amino)-4-nitroazobenzene)], and then the sample was post-poled using a high dc electric field in a wire-poling scheme.[14,15] The poling was thermally assisted by heating the film to near the polymer glass transition temperature. By slowly cooling the film down to room temperature while keeping the electric field, the molecular orientations can be maintained in a noncentrosymmetric arrangement.[16] However, the nonlinear optical properties varied significantly, depending on the amplitude of the surface relief modulation and on the diffraction efficiency of the initial grating, and in addition, new half-period structures were observed in the higher diffraction gratings.[15]

From a fundamental point of view, it is very important to characterize the molecular orientations of the active nonlinear optical (NLO) chromophores after a poling process.[14,16,17] The mapping of the spatially resolved molecular orientations in the different regions of the mesostructure using polarized measurements in the linear and nonlinear optical regimes can then be correlated with the optical properties of the polar grating.

The main goals of this study are to determine the molecular orientations of azobenzene chromophores in the various regions of a sinusoidal surface grating and to establish their corresponding most probable orientational distribution functions. More precisely, using both confocal Raman microscopy and second harmonic generation near-field scanning optical microscopy (SHG-NSOM),[18] we have determined for the first time the first four Legendre order parameters $\langle P_1 \rangle$, $\langle P_2 \rangle$, $\langle P_3 \rangle$, and $\langle P_4 \rangle$ and

* To whom correspondence should be sent. E-mail: f.lagugne@lpcm.u-bordeaux1.fr.

10.1021/jp047117k CCC: $27.50
Published on Web 10/07/2004

SCHEME 1

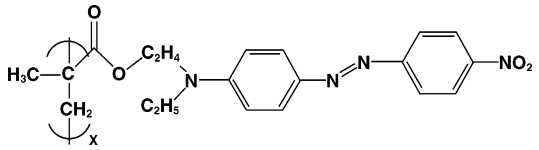

the associated distribution functions in the bottom, midslope, and peak regions of a polymer thin grating. These techniques are quite complementary since Raman spectroscopy is sensitive to the even parity order parameters, $\langle P_2 \rangle$ and $\langle P_4 \rangle$, while second-order nonlinear techniques like SHG or SFG (sum frequency generation) are sensitive to the odd parity order parameters, $\langle P_1 \rangle$ and $\langle P_3 \rangle$. It is noteworthy that the latter parameters describe all polar ordering of the molecules oriented at surfaces, interfaces and/or in any noncentrosymmetric materials.[19−21] All four order parameters obtained independently from polarized Raman spectroscopy[22−24] and polarized SHG measurements[25] can be associated with the intrinsic orientation of any particular dipole. The knowledge of the $\langle P_l \rangle$ factors then leads to the distribution functions, $f(\langle P_l \rangle)$, that precisely describe the chromophore orientations in the different regions of the surface relief grating. Since the microscopic techniques have a different lateral spatial resolutions (∼500 nm in Raman microscopy; ∼100 nm in NSOM), the grating spacing was chosen to be about 1.4 μm, i.e., large enough to be scanned with accuracy and reproducibility in both the far-field confocal and near-field microscopies.

The paper is organized as follows: In the Experimental Section (section II), the grating inscription and poling procedure of the azopolymer thin films are described. Some details about the experimental setups of confocal micro-Raman and SHG-NSOM are reported. In section III, the approaches used to measure the order parameters are extensively described and theoretical expressions are derived for both techniques. Corrections to the scattered intensity from the high numerical aperture objective lens are considered in the confocal Raman measurements and, corrections from Fresnel factors are taken into account in the SHG-NSOM measurements. Finally, the distribution functions $f(\langle P_1 \rangle, \langle P_2 \rangle, \langle P_3 \rangle, \langle P_4 \rangle)$ are derived using the information entropy model, and the most probable distributions, in particular at the top and bottom regions of the grating, are compared.

This work completes previous Raman[26] and SHG-NSOM[15] studies of these nonlinear gratings and it establishes for the first time the most probable orientation distribution functions associated with the azobenzene chromophores in a noncentrosymmetric mesostructured material.

II. Experimental Section

II.A. Materials and Grating Inscription. The gratings were inscribed on thin films of the p(DR1M) homopolymer, (Scheme 1). Thin films were prepared by spin casting (1500 rpm) a solution of p(DR1M) (5 wt %) in chloroform onto clean microscope slides. The thickness of the films was determined by contact mode atomic force microscopy (AFM) and was equal to 400 ± 10 nm. The holographic setup developed for the grating inscription using horizontally polarized (p + p) interfering beams consisted of a two arm interferometer that generates an interference pattern.[27] A single argon laser beam (λ = 514.5 nm) was first expanded using a spatial filter (pinhole 25 μm, ×10 objective). An additional microscope objective was used to obtain a parallel and homogeneous spot with a 3 mm diameter. The beam was then circularly polarized and passed through a Wollaston prism in order to generate two beams with

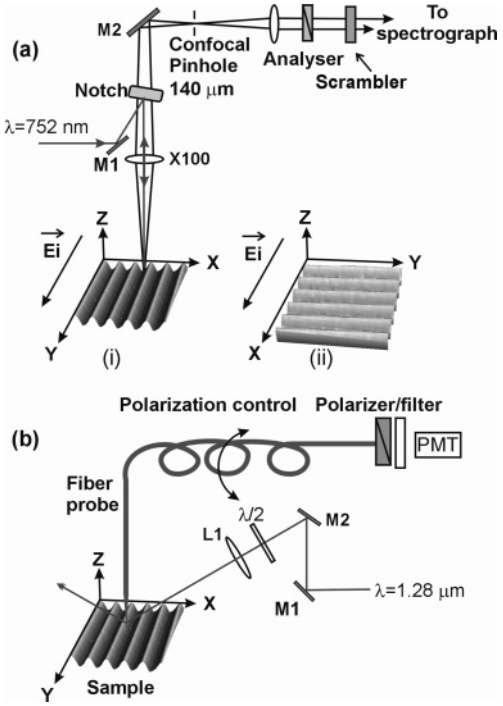

Figure 1. (a) Experimental setup for the polarized micro-Raman. Since the input polarization is fixed, the (*YY*) and (*YX*) spectra are recorded using the (i) geometry while (*XX*) and (*XY*) are recorded in the (ii) configuration. (b) SHG-NSOM setup. The input/output polarization can be selected using a half-waveplate and a glan polarizer, respectively.

p (horizontal) and s (vertical) polarizations, respectively. The polarizations of the two emerging beams were then adjusted to p polarization using a half-wave retarder. For each beam, the degree of polarization was always better than 98%, and the irradiance was equal to ∼50 mW/cm^2. The beams were then recombined onto the sample free surface with an incidence angle of ∼11°, which corresponds to a grating period of 1.37 μm. The diffraction efficiency of the grating was monitored during the fabrication allowing the in situ control of the grating formation. In the present study, we have prepared several gratings with medium (η = 12%) and high diffraction efficiencies (η = 25%). Once the gratings are fabricated, electrical poling is performed using a wire poling scheme. This process gives rise to an efficient and permanent polar ordering of the azobenzene chromophores, provided it is done in the dark in three steps: First, the thin film is annealed to 90 °C (∼20 °C below the glass transition temperature). Second, when this temperature is reached, a 3 kV voltage is applied between the film and a tungsten wire located 5 mm above the film, and this potential is maintained for 1 h at 90 °C. Finally, to freeze the polar orientation of the chromophores, the sample is cooled to room temperature at 1 °C/min with the potential still applied. Linear (UV−visible) and nonlinear (SHG) optical measurements have shown that this poling method is very efficient: we have observed temporally stable large values of the d_{33} nonlinear coefficient that vary from 200 to 300 pm/V, even after a 3 month period of relaxation. Besides, we have also noted a higher remnant polar orientation when the dc potential was applied for a longer time (2 h). More details about the far-field polarized SHG measurements can be found elsewhere.[17,24]

II.B. Confocal Raman Measurements. The Raman spectra were recorded in a backscattering geometry on a Labram I instrument (Jobin-Yvon, Horiba group, France) and a 100× (NA = 0.9) objective lens (Figure 1a). The input polarization was

fixed while polarization analysis of the scattered signal was selected using a polarizing analyzer and scrambler before the entrance slit of the spectrometer. Laser irradiations were performed at $\lambda = 752.5$ nm (Kr^+) with a low power, $I = 0.75$ to 1.5 mW, to avoid any bleaching or thermal degradation of the sample. Scanning of the sample was performed using a *XY* motorized table. Typically, several 5-μm-long lines were scanned with 0.125 μm resolution, which corresponded to 40 spectra per line. Each Raman spectrum was integrated over 10 s. Data were averaged over three lines, leading to a total acquisition time of about 20 min for the recording of a polarized Raman image. More technical details about the confocal Raman microscopy setup can be found in previous publications by our group.[22−26]

II.C. Second Harmonic Generation Near-Field Scanning Optical Microscopy. SHG-NSOM experiments were conducted in collection mode using a commercial NSOM apparatus (Thermomicroscope, Veeco, Lumina). This instrument is equipped with a shear-force feedback mechanism that maintains a constant sample−tip separation of about 5 nm, which also provides a topographical image of the sample. As shown in Figure 1b, femtosecond laser pulses were focused from the far-field to a $\sim(100\ \mu m)^2$ spot in a region of the sample that is investigated by the near-field probe. Signals collected in the near-field were directed by a single mode fiber optics to a filter and a glan polarizer before detection by a photomultiplier (Hamamatsu R300) in conjunction with a boxcar integrator. In the present study, homemade noncoated tips were fabricated using a standard etching procedure with hydrofluoric acid (45%). Noncoated probes were used, as these are more appropriate for nonlinear optical measurements, since any metallic coating would induce significant perturbations to optical processes because of the high polarizability of the metal.[28,29] The light source for the measurements consisted in a Ti:sapphire oscillator (800 nm, 480 mW, 30 fs, 88 MHz) which was used to seed a commercial chirped pulse amplifier (800 nm, 2.25 W, 80 fs, 1 kHz). This output was used to pump a commercial superfluorescence optical parametric amplifier (OPA), the wavelength of which being tuned from 1.1 to 2.7 μm. In the experiments reported hereafter, the fundamental wavelength was fixed at 1.28 μm and the second harmonic signal was detected at 0.64 μm. The sample was scanned using a piezoelectric stage within a range of 50 μm × 50 μm in the $X-Y$ plane and of 10 μm along the *Z* direction. In a typical experiment we have scanned $(10\ \mu m)^2$ regions of the grating. This represented 200 × 200 points and the corresponding image with polarization analysis was recorded in about 30 min. Details of the setup can be found elsewhere. [30−33]

III. Determination of the Four First Orientational Order Parameters

In the present study, we focus on a grating with a 25% diffraction efficiency and a sinusoidal surface relief modulation of about 390 nm amplitude, which is nearly equal to the initial thickness of the film. Indeed, the grating was inscribed using the very efficient (p + p) polarization configuration, which leads to highly diffractive gratings.[34] In such a polarization configuration, the resulting optical field from the interference pattern is always polarized along the horizontal direction, i.e. perpendicular to the grating grooves, as shown in Figure 2.a; this implies that the final molecular orientations of the chromophores are expected to be in the perpendicular directions after numerous trans−cis−trans isomerization cycles. Assuming a uniaxial photoinduced reorientation of the rodlike molecules with respect to the actinic optical field, the azobenzene entities will have the same probability to orient in the "in-plane" (*Y*) and "out-of-plane" (*Z*) equivalent directions (Figure 2b). This is quite important since we must know accurately the order parameters in the "out-of plane" direction in order to get a complete set of the orientation factors, including the odd order parameters. The uniaxial approximation is also valid for the poling process but the reference direction is now normal to the film plane. In this uniaxial model, the orientations of the molecules of cylindrical symmetry (the molecules have a rotational symmetry along their long molecular axis) can be described by a unique polar θ angle between the molecular director and the "out-of-plane" Z direction. Under these assumptions, the angular distribution functions $f(\theta)$ can be developed on the basis of the Legendre polynomials:

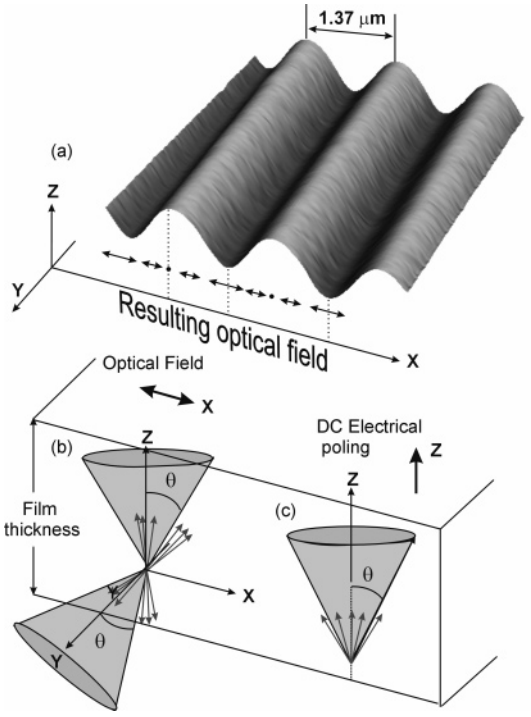

Figure 2. Components of the incident optical field upon grating inscription using the (p + p) polarization configuration of the interfering beams (a). Angular distribution of the azo-chromophores relative to the reference directions. For Raman measurements, the chromophores undergo angular reorientation along the *Y* and *Z* directions (b). For nonlinear optical measurements, the reference direction is normal to the film plane (c), and the dipoles are oriented asymmetrycally (polar orientation) along *Z*.

$$\langle n_T \rangle = \frac{N}{8\pi^2}\int_0^{2\pi} d\psi \int_0^{2\pi} d\varphi \int_{-1}^{+1} f(\theta)\, d(\cos\theta) \qquad (1)$$

with

$$f(\theta) = \sum_{l=0}^{\infty}\left(l + \frac{1}{2}\right)\langle P_l\rangle P_l(\cos\theta) \qquad (2)$$

where the coefficients $\langle P_l\rangle$ are given by

$$\langle P_l\rangle = \int_0^{\pi} P_l(\cos\theta)\, f(\theta)\, \sin\theta\, d\theta \qquad (3)$$

with

$$\langle P_0\rangle = 1.0$$

$$\langle P_1\rangle = \langle \cos\theta\rangle$$

$$\langle P_2\rangle = \frac{1}{2}(3\langle \cos^2\theta\rangle - 1)$$

$$\langle P_3\rangle = \frac{1}{2}(5\langle \cos^3\theta\rangle - 3\langle \cos\theta\rangle)$$

$$\langle P_4\rangle = \frac{1}{8}(35\langle \cos^4(\theta)\rangle - 30\langle \cos^2(\theta)\rangle + 3) \quad (4)$$

From eq 2 the resulting distribution function can be derived knowing the $\langle P_l\rangle$ values but, of course, the series will be truncated and not necessarily converging. As discussed in the literature, it is more accurate to determine the most probable orientational distribution function $f(\theta)$ in the framework of the information entropy theory using the order parameter values measured by polarized Raman scattering,[24,35,36] and by second-order NLO experiments.[37−39] Actually, in this general approach, the distribution function is obtained by maximizing the information entropy, and the Lagrange method of undetermined multipliers leads to the normalized function which includes the four first orientation parameters:[35,36,40−43]

$$f(\theta) = \frac{\exp(\lambda_1 P_1(\cos\theta) + \lambda_2 P_2(\cos\theta) + \lambda_3 P_3(\cos\theta) + \lambda_4 P_4(\cos\theta))}{\int_{-1}^{+1} \exp(\lambda_1 P_1(\cos\theta) + \lambda_2 P_2(\cos\theta) + \lambda_3 P_3(\cos\theta) + \lambda_4 P_4(\cos\theta))\, \mathrm{d}(\cos\theta)} \quad (5)$$

where the Lagrange multipliers λ_1, λ_2, λ_3, and λ_4 are numerically calculated using eq 3 for each $\langle P_l\rangle$ parameter.

Therefore, from the experimentally determined $\langle P_2\rangle$ and $\langle P_4\rangle$ from micro-Raman experiments and $\langle P_1\rangle$ and $\langle P_3\rangle$ from SHG-NSOM measurements, one can estimate all of the λ_1, λ_2, λ_3, and λ_4 multipliers. From application of the general information entropy model (eq 5) the most probable normalized and physically meaningful distribution functions, $f(\theta)$, can be derived for any surface relief region of the diffraction grating.

III.A. Raman Measurements and Estimation of $\langle P_2\rangle$ and $\langle P_4\rangle$. The theoretical approach of polarized Raman intensities taking into consideration the use of a large NA microscope objective has been already considered for gratings inscribed with the (p + p) interference pattern.[23,24] We recall here the essential expressions to obtain $\langle P_2(\cos\theta)\rangle$ and $\langle P_4(\cos\theta)\rangle$ and we must underline that in previous studies the two first even order parameters were determined relative to the actinic field polarization direction, i.e., along the *X* axis for the (p + p) configuration. Here, to compare the orientation parameter values with the nonlinear optical results, a common axis corresponding to either the *Z* or *Y* direction must be selected as a proper reference axis.

Polarized Raman intensities depend on averaging over all orientations in space,

$$I_{IJ} \propto \langle \alpha_{IJ}{}^2 n_T\rangle \quad (6)$$

where *I, J* denote the input and analyzer polarizations, respectively, and α_{IJ} are the molecular polarizability tensor elements:

$$\langle \vec{\alpha}_{IJ}{}^2 n_T\rangle = \int_0^{2\pi} \mathrm{d}\psi \int_0^{2\pi} \mathrm{d}\varphi \int_{-1}^{+1} n_T(\theta)[T(\theta,\varphi,\psi)\ \alpha\ T^t(\theta,\varphi,\psi)]^2\, \mathrm{d}(\cos\theta) \quad (7)$$

where T and T^t are the normal and transposed classical Euler matrices, respectively. Since the integral over the angle θ is only considered, the averaged quantities $\langle \alpha_{IJ}{}^2\rangle$ can be expressed in terms of $\langle \cos^2\theta\rangle$ and $\langle \cos^4\theta\rangle$, i.e., in terms of $\langle P_2\rangle_Z$ and $\langle P_4\rangle_Z$. Furthermore, in a rigorous treatment, the use of a high numerical aperture objective must be taken into account. Using the results of eq 7 and the scattering geometry with the grating grooves oriented along the polarization direction of the input beam (along *Y*), in a first set of experiments we may record the two spectra corresponding to the following intensity equations:

$$I_{YX} = [\langle \alpha_{YX}{}^2\rangle A + \langle \alpha_{YZ}{}^2\rangle B](2C_0 + C_2) + [\langle \alpha_{ZX}{}^2\rangle A + \langle \alpha_{ZZ}{}^2\rangle B]](4C_1) + [\langle \alpha_{XX}{}^2\rangle A + \langle \alpha_{XZ}{}^2\rangle B]C_2 \quad (8)$$

$$I_{YY} = [\langle \alpha_{YY}{}^2\rangle A + \langle \alpha_{YZ}{}^2\rangle B](2C_0 + C_2) + [\langle \alpha_{ZY}{}^2\rangle A + \langle \alpha_{ZZ}{}^2\rangle B](4C_1) + [\langle \alpha_{XY}{}^2\rangle A + \langle \alpha_{XZ}{}^2\rangle B]C_2 \quad (9)$$

In a second set of experiments, the grating is 90° rotated under the microscope stage with its grooves oriented in the direction perpendicular to the input beam polarization. We then record the two other polarized spectra:

$$I_{XY} = [\langle \alpha_{XY}{}^2\rangle A + \langle \alpha_{XZ}{}^2\rangle B](2C_0 + C_2) + [\langle \alpha_{ZY}{}^2\rangle A + \langle \alpha_{ZZ}{}^2\rangle B](4C_1) + [\langle \alpha_{YY}{}^2\rangle A + \langle \alpha_{YZ}{}^2\rangle B]C_2 \quad (10)$$

$$I_{XX} = [\langle \alpha_{XX}{}^2\rangle A + \langle \alpha_{XZ}{}^2\rangle B](2C_0 + C_2) + [\langle \alpha_{ZX}{}^2\rangle A + \langle \alpha_{ZZ}{}^2\rangle B](4C_1) + [\langle \alpha_{YX}{}^2\rangle A + \langle \alpha_{YZ}{}^2\rangle B]C_2 \quad (11)$$

Here, the quantities A (2.9685) and B (0.4956) come from integration of the squares of the electric vector components over the scattering cone and the constants $C_0 = 5.3825$, $C_1 = 0.1424$, and $C_2 = 5 \times 10^{-4}$ are related to the focalization efficiency; they were calculated via integration of the incident electric field vector components over the effective irradiated volume.[44] All these parameters are dependent on the angular semiaperture of the objective ($\theta = 64.16°$ for the ×100, NA = 0.9, microscope objective) and on the refractive index of the sample ($n = 1.645$). Finally, from the knowledge of the relative intensities $I_{IJ}(\delta)$ in the different parts ($\delta = 2\pi X/(\text{period})$) of the grating and, more precisely of their ratios $R_1(\delta) = I_{XY}/I_{XX}$ and $R_2(\delta) = I_{YX}/I_{YY}$, the two first even order parameter values of $\langle P_2\rangle$ and $\langle P_4\rangle$ can be estimated.

As shown in Figure 3, the Raman spectra were investigated in the 700−1700 cm^{-1} spectral domain; for instance, the two couples of (*YY*) and (*YX*) polarized spectra display strong and similar intensity variations for various Raman signals confirming the existence of important orientational effects. In particular, the spectra exhibit intense signals at 1104 (ν(Φ−N), 18a), 1134 and 1196 cm^{-1} (δ(CH) ring, 9a and 9b), 1336 cm^{-1} ($\nu_s(NO_2)$), 1392 cm^{-1} (ν(N═N)), 1422 and 1447 cm^{-1} (δ(CH) ring, 19a and 19b), 1572 and 1589 cm^{-1} (ω(C═C), 8a and 8b) characteristic of the "trans" azobenzene chromophore.[24] In the following we have arbitrarily selected the whole 1044−1180 cm^{-1} spectral range to calculate the intensity integrations and their ratio. As illustrated in Figure 4, parts a and b, we have thus obtained the polarized Raman images over a (5 μm)^2 area for *YY* and *YX* polarizations, respectively. Under these conditions, the variations over several grating periods of the average polarized Raman intensities are plotted on Figure 5, parts a and b for the full set of input/output polarizations. Note that integrations of the single band ν_s NO_2 at 1336 cm^{-1} would give

TABLE 1: Values of the Order Parameters $\langle P_1\rangle$, $\langle P_2\rangle$, $\langle P_3\rangle$, and $\langle P_4\rangle$ and Their Associated Lagrange Multipliers According to the Information Entropy Theory in the Tops and Bottoms of a Grating Inscribed on P(DR1M) Polymer[a]

position ($\delta = 2\pi X$/period)	$R_1(\delta)$	$R_2(\delta)$	$\langle P_2\rangle$	$\langle P_4\rangle$	λ_2	λ_4	function type
0.0 bottoms	0.701	0.307	0.228	−0.067	1.273	−0.837	bimodal asymmetric
intermediate	0.873	0.3485	0.251	−0.153	1.727	−1.815	bimodal symmetric
$\Lambda/2$ (tops)	1.045	0.390	0.266	−0.230	2.070	−2.829	bimodal symmetric

position	$d_{33\ \mathrm{pm/V}}$	$d_{31\ \mathrm{pm/V}}$	$\langle P_1\rangle$	$\langle P_3\rangle$	λ_1	λ_3	function type
0.0	15.7	4.44	0.085	0.004	0.256	0.027	polar asymmetric
intermediate	62.1	9.24	0.277	0.121	0.807	0.737	polar asymmetric
$\Lambda/2$ (tops)	44.4	7.21	0.201	0.072	0.597	0.464	polar asymmetric

position	$\langle P_1\rangle$, λ_1	$\langle P_2\rangle$, λ_2	$\langle P_3\rangle$, λ_3	$\langle P_4\rangle$, λ_4	function type
0.0	0.085, 0.182	0.223, 1.228	0.004, −0.040	−0.067, −0.847	polar asymmetric, very broad max ±34°
intermediate	0.277, 0.727	0.251, 1.251	0.121, 1.297	−0.153, −2.429	polar asymmetric, broad max ±35°
$\Lambda/2$	0.201, 0.502	0.266, 2.123	0.072, 0.987	−0.230, −3.511	polar asymmetric, max ±35°

[a] The distribution functions are first developed separately using the Raman result and the SHG results and finally expressed considering the full set of order parameters.

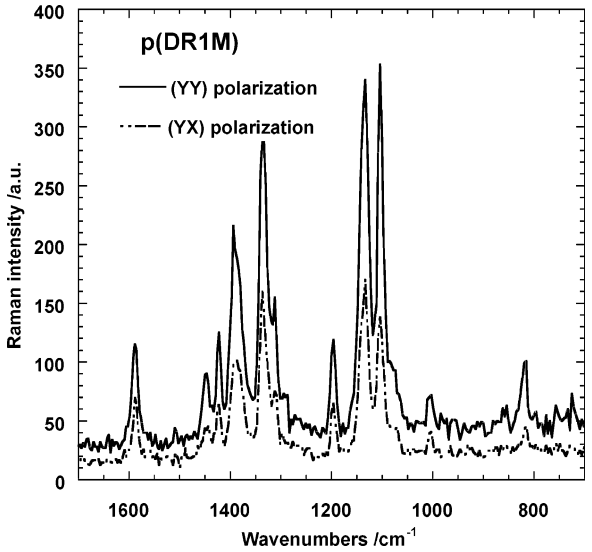

Figure 3. Typical polarized Raman spectra of a p(DR1M) electrically poled grating in the 700−1700 cm^{-1} spectral range.

rise to similar results, but with a poorer signal-to-noise ratio. Consequently, the values of $R_1(\delta)$, $R_2(\delta)$, $\langle P_2\rangle$, and $\langle P_4\rangle$ can be derived in the various regions (bottoms, intermediates, tops) of the surface relief of the diffraction grating. Corresponding values are reported in Table 1 and the curve variations of $\langle P_2\rangle$ and $\langle P_4\rangle$ are plotted in Figure 6. The Lagrange multipliers λ_2 and λ_4 and their associated distribution functions (see Table 1) are then determined within the information entropy theory when considering only the Raman results, i.e. stating $\langle P_1\rangle = 0, \langle P_3\rangle = 0$.

III.B. SHG-NSOM Measurements and Estimation of $\langle P_1\rangle$ and $\langle P_3\rangle$. In the following we have considered a $C_{\infty v}$ symmetry of the rodlike molecules that are noncentrosymmetrically oriented in the poled thin film. Under this assumption, from SHG polarized measurements one can get estimates of the susceptibilities and nonlinear coefficients d_{33}, d_{31}, and d_{15} which are used to determine the two orientational odd order parameters $\langle P_1(\cos\theta)\rangle$ and $\langle P_3(\cos\theta)\rangle$.

III.B.1. Theory for a Material with Bulk Nonlinearity and $C_{\infty v}$ Symmetry. In this approach, only three independent elements are effective, namely $\chi_{zzz} = \chi_{33} = 2d_{33}$, $\chi_{xzx} = \chi_{yzy} = \chi_{xxz} = \chi_{yyz} = \chi_{15} = 2d_{15}$, and $\chi_{zxx} = \chi_{zyy} = \chi_{31} = 2d_{31}$. In experiments carried out under reflection mode, the effective susceptibilities can be written for the three adequate polarization configurations (P_{in}, P_{out}), (S_{in}, P_{out}) and ($+45°_{in}/S_{out}$):

$$\chi_{\mathrm{eff}}^{\mathrm{PP}} = (L_z^2(\omega)L_z(2\omega)\sin^3\beta)\chi_{33} - (2L_x(\omega)L_x(2\omega)L_z(\omega) \times \cos^2\beta\sin\beta)\chi_{15} + (L_x^2(\omega)L_z(2\omega)\cos^2\beta\sin\beta)\chi_{31}$$

$$\chi_{\mathrm{eff}}^{\mathrm{SP}} = (L_y^2(\omega)L_z(2\omega)\sin\beta)\chi_{31}$$

$$\chi_{\mathrm{eff}}^{45/\mathrm{S}} = (L_y(\omega)L_y(2\omega)L_z(\omega)\sin\beta)\chi_{15} \qquad (12)$$

where β is the angle of incidence of the fundamental beam ($\beta = 60°$) and $L_i(\omega)$ and $L_i(2\omega)$ are the Fresnel factors at the fundamental and second harmonic wavelengths, respectively.[45] In the calculations, we have made use of the index of refraction $n = 1.624$ at 1.064 μm ($n = 1.700$ at 532 nm) and of the Fresnel coefficients $L_x = 1.020$ (1.001), $L_y = 0.533$ (0.509), and $L_z = 0.371$ (0.344) at the fundamental (second harmonic) wavelength. From these parameter values, we obtain the coherence length $l_c = 29.8$ nm for the azobenzene material and the following relations:

$$\chi_{\mathrm{eff}}^{\mathrm{PP}} = (0.0308)\chi_{33} - (0.1651)\chi_{15} + (0.0775)\chi_{31}$$

$$\chi_{\mathrm{eff}}^{\mathrm{SP}} = (0.0848)\chi_{31}$$

$$\chi_{\mathrm{eff}}^{45/\mathrm{S}} = (0.0874)\chi_{15} \qquad (13)$$

From the two latter expressions of the susceptibilities it can be readily checked that the assumption $\chi_{31} = \chi_{15}$ is justified. Also, from all the polarized SHG data of the poled azobenzene sample, we can get estimates of the tensor elements d_{33}, d_{31} (d_{15}) in the various parts of a grating. For this purpose we have used a ZnSe reference crystal ($d_{14} = 27$ pm/V), and the complete susceptibility expressions for this crystal with the corresponding normalized expressions are reported in the Appendix.[46]

III.B.2. Polarization Measurements in SHG-NSOM.. Typical SHG-NSOM images obtained from scans over a (5 × 5) μm^2 area are shown in Figure 4, parts c and d, which display topography and SHG optical contrast, respectively. The corresponding polarized SHG variations averaged over 20 lines are reported in Figure 7a for PP and SP configurations. Similar polarized measurements were recorded for the reference ZnSe crystal under the same conditions and were averaged over 2000 laser shots for both PP and SP polarizations. After

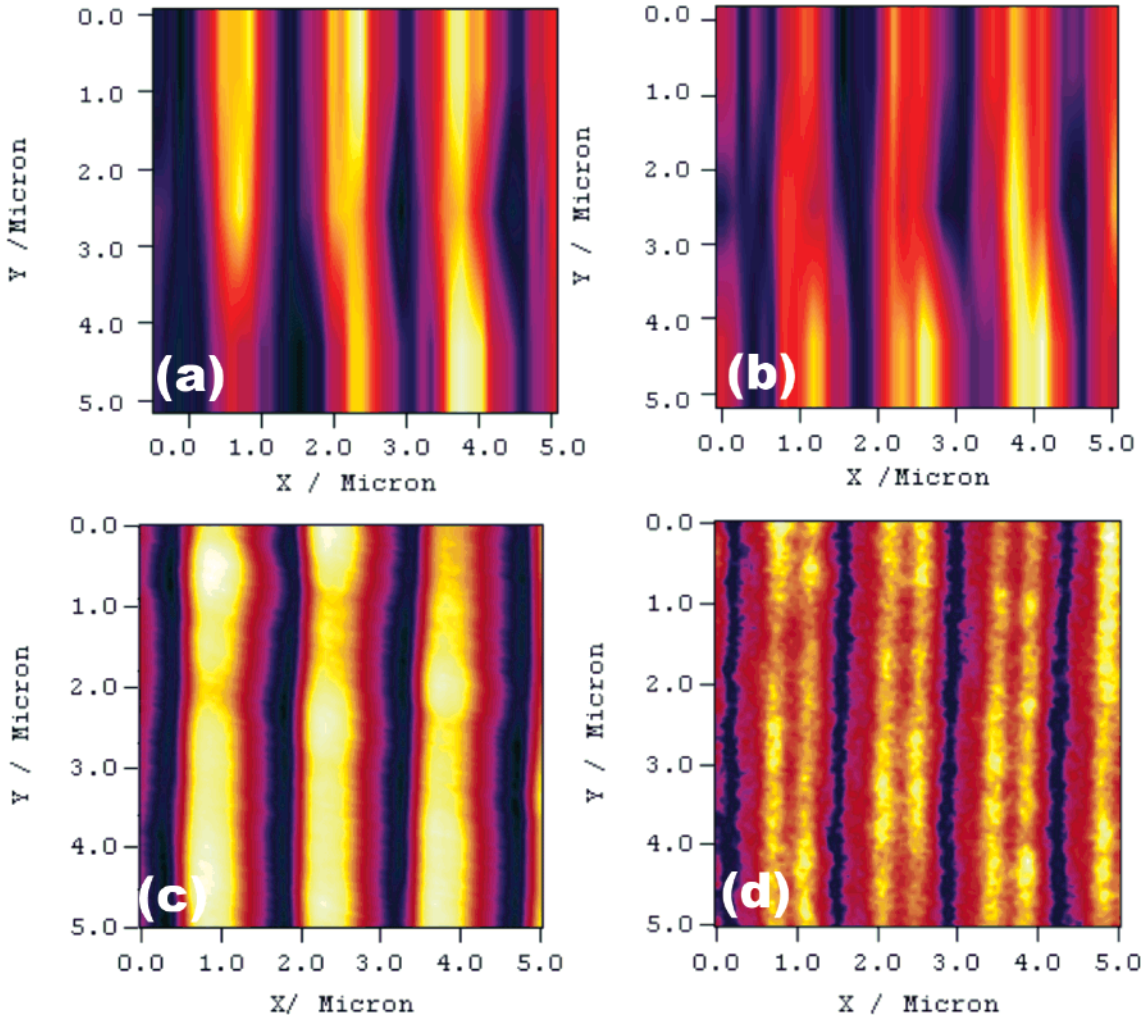

Figure 4. Polarized Raman images under (a) the (*YY*) and (b) the (*YX*) polarization conditions. Near-field scanning images of the topography (c) and the SHG contrast (d).

normalization with ZnSe, eq 13 can be rewritten:

$$|\chi_{\text{eff}}^{\text{PP}}(\text{Azo})| = (0.0308\chi_{33} - 0.1651\chi_{15} + 0.0775\chi_{31}) = \frac{1.94.10^{-20}}{l_c(\text{Azo})}\sqrt{\frac{I^{\text{PP}}(\text{Azo})}{I^{\text{PP}}(\text{ZnSe})}}$$

$$|\chi_{\text{eff}}^{\text{SP}}(\text{Azo})| = (0.0848)\chi_{31} = \frac{1.836.10^{-20}}{l_c(\text{Azo})}\sqrt{\frac{I^{\text{SP}}(\text{Azo})}{I^{\text{SP}}(\text{ZnSe})}} \quad (14)$$

Taking $\chi_{31} \equiv \chi_{51}$ (or equivalently $2d_{31} \equiv 2d_{15}$), we finally arrive at a system of two equations with two unknown coefficients d_{31} and d_{33}:

$$d_{33} = 1.057.10^{-11}\sqrt{\frac{I^{\text{PP}}(\text{Azo})}{I^{\text{PP}}(\text{ZnSe})}} + (0.286)d_{31}$$

$$d_{31} = 3.63.10^{-12}\sqrt{\frac{I^{\text{SP}}(\text{Azo})}{I^{\text{SP}}(\text{ZnSe})}} \quad (15)$$

As shown in Figure 7b, values of the d_{33} coefficient in the grating are found to vary from ~16 pm/V in the bottom positions to ~44 pm/V in the top positions, and they show maxima of about 62 pm/V in the intermediate surface regions. It is noteworthy that the latter value is ~2 times larger than d_{14} in crystalline ZnSe and ~20 times larger than the d_{11} value in

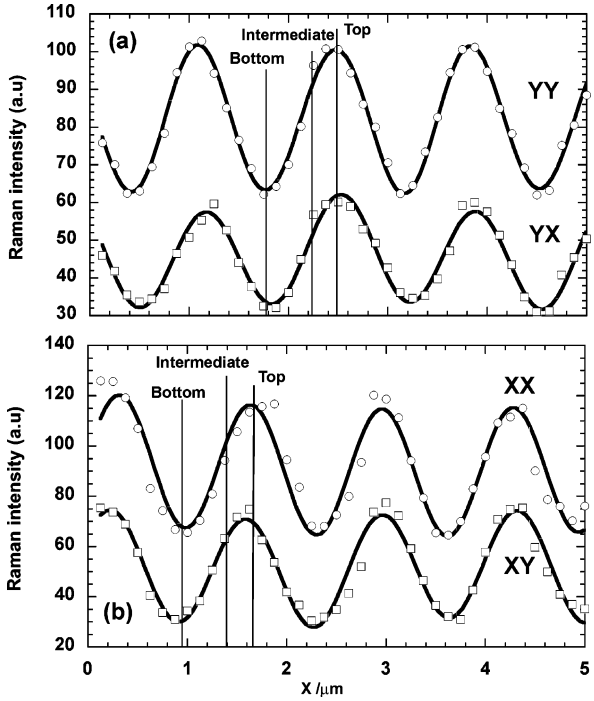

Figure 5. Set of polarized Raman intensities integrated over the 1044−1180 cm^{-1} spectral range: (a) *YY* and *YX* polarizations; (b) *XX* and *XY* polarizations. The solid curves are guides to the eye.

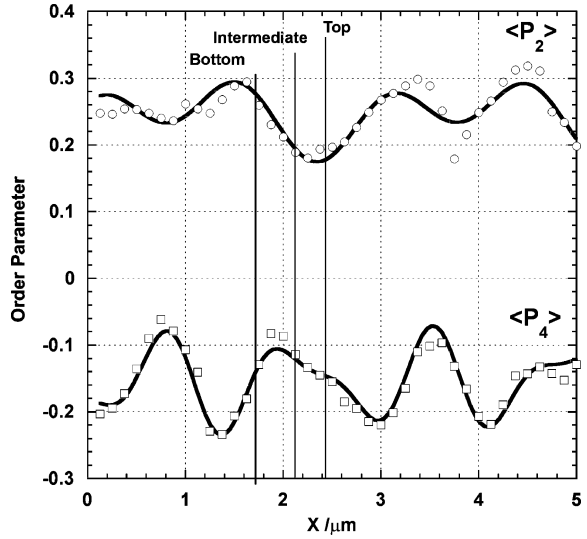

Figure 6. Variation of $\langle P_2 \rangle$ and $\langle P_4 \rangle$ along the grating vector. The solid curves are guides to the eye.

α-quartz.[17,47] However, in conventional far-field experiments, even higher values of about 200−300 pm/V have been observed in transmission SHG measurements on flat surfaces of the poled polymer film in the vicinity of the inscribed grating.[17]

Actually, from the real parts of the d_{33} and d_{31} coefficients we can now extract the order parameters that characterize the polar ordering of the azobenzene molecules. As developed by Kuzyk and Singer,[48] the susceptibilities can be expressed in terms of $\langle P_1 \rangle$ and $\langle P_3 \rangle$:

$$\chi_{33} = 2d_{33} = N\beta_{zzz}\left(\frac{3}{5}\langle P_1 \rangle + \frac{2}{5}\langle P_3 \rangle\right)$$

$$\chi_{31} = 2d_{31} = N\beta_{zzz}\left(\frac{1}{5}\langle P_1 \rangle - \frac{1}{5}\langle P_3 \rangle\right) \qquad (16)$$

In the DR1 azobenzene rodlike molecule, the molecular hyperpolarizability, β_{zzz}, along the z axis (the main molecular axis) is only dominant. From literature data,[47,48] we have assumed $\beta_{zzz} = 586 \times 10^{-12}$ m/V and we have finally calculated the $\langle P_1 \rangle$ and $\langle P_3 \rangle$ values and followed their variations over several periods in the different parts of the surface relief grating (Figure 8) by using the following expressions:

$$\langle P_1 \rangle = \frac{4(d_{33} - 2d_{31})}{N\beta_{zzz}}$$

$$\langle P_3 \rangle = \frac{4(d_{33} - 3d_{31})}{N\beta_{zzz}} \qquad (17)$$

III.C. Results and Discussion. To point out the influence of the even and odd order parameters, we have first derived, compared, and then plotted the distribution functions in polar coordinates under various assumptions: (i) using only the even order parameters, $\langle P_2 \rangle$ and $\langle P_4 \rangle$, (Figure 9a−c), (ii) using only the odd order parameters $\langle P_1 \rangle$ and $\langle P_3 \rangle$ (Figure 9d−f), and (iii) finally, using a complete set of the even and odd Legendre polynomials (Figure 9g−i).

All the order parameter values and associated Lagrange multipliers are gathered in Table 1.

(i) First, the $\langle P_2 \rangle$ order parameter varies from +0.228 (bottoms) to +0.266 (tops). As expected, these values are positive, but they denote an orientational ordering along the Z reference direction which is far from being perfect. For a perfect

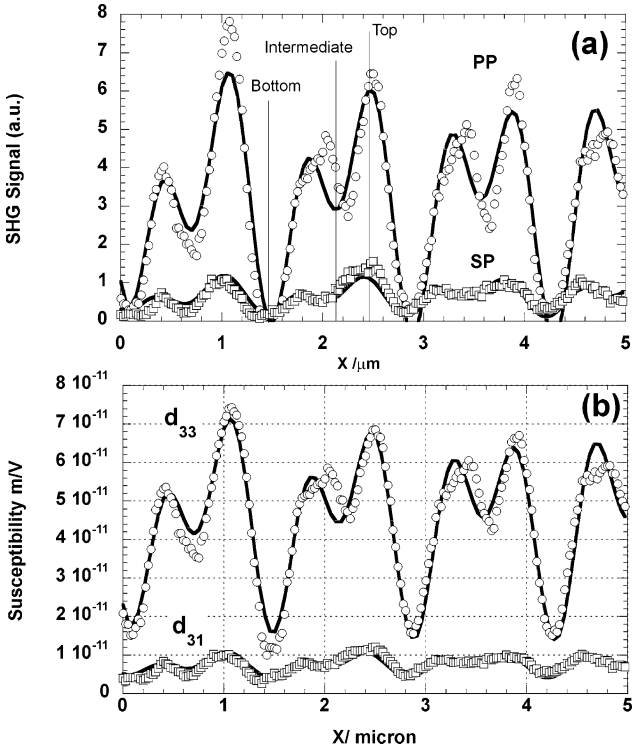

Figure 7. (a) SHG-NSOM profiles of the surface relief grating with PP and SP polarizations. (b) Variation of the susceptibility elements d_{33} and d_{31} along the grating period. The solid curves are guides to the eye.

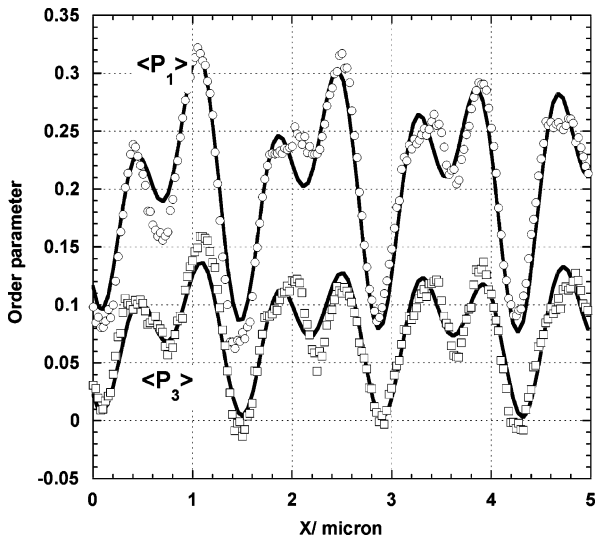

Figure 8. Variations of the order parameters $\langle P_1 \rangle$ and $\langle P_3 \rangle$ along the grating period. The solid curves are guides to the eye.

alignment one should expects $\langle P_2 \rangle = 1.0$. However, it is noteworthy that these $\langle P_2 \rangle$ values agree well with the +0.225 estimate obtained from UV−visible transmission measurements recorded on the same poled films in the near vicinity of the grating location.[24] In contrast, the parameter $\langle P_4 \rangle$ is always negative and varies markedly from −0.067 (bottoms) to −0.230 (tops): the influence of $\langle P_4 \rangle$ is thus preponderant on the shape of distribution function. Actually, using only the sets of $\langle P_2 \rangle$, $\langle P_4 \rangle$, the distribution functions are asymmetric and display maxima at ±34° (bottoms), ±39° (intermediates), and ±42° (tops) with respect to the direction of reference. Also, the distribution function in the top regions is significantly narrower than in the bottoms regions (the full width at half-maximum, fwhm, varies from ∼28 to ∼60°); this probably indicates the

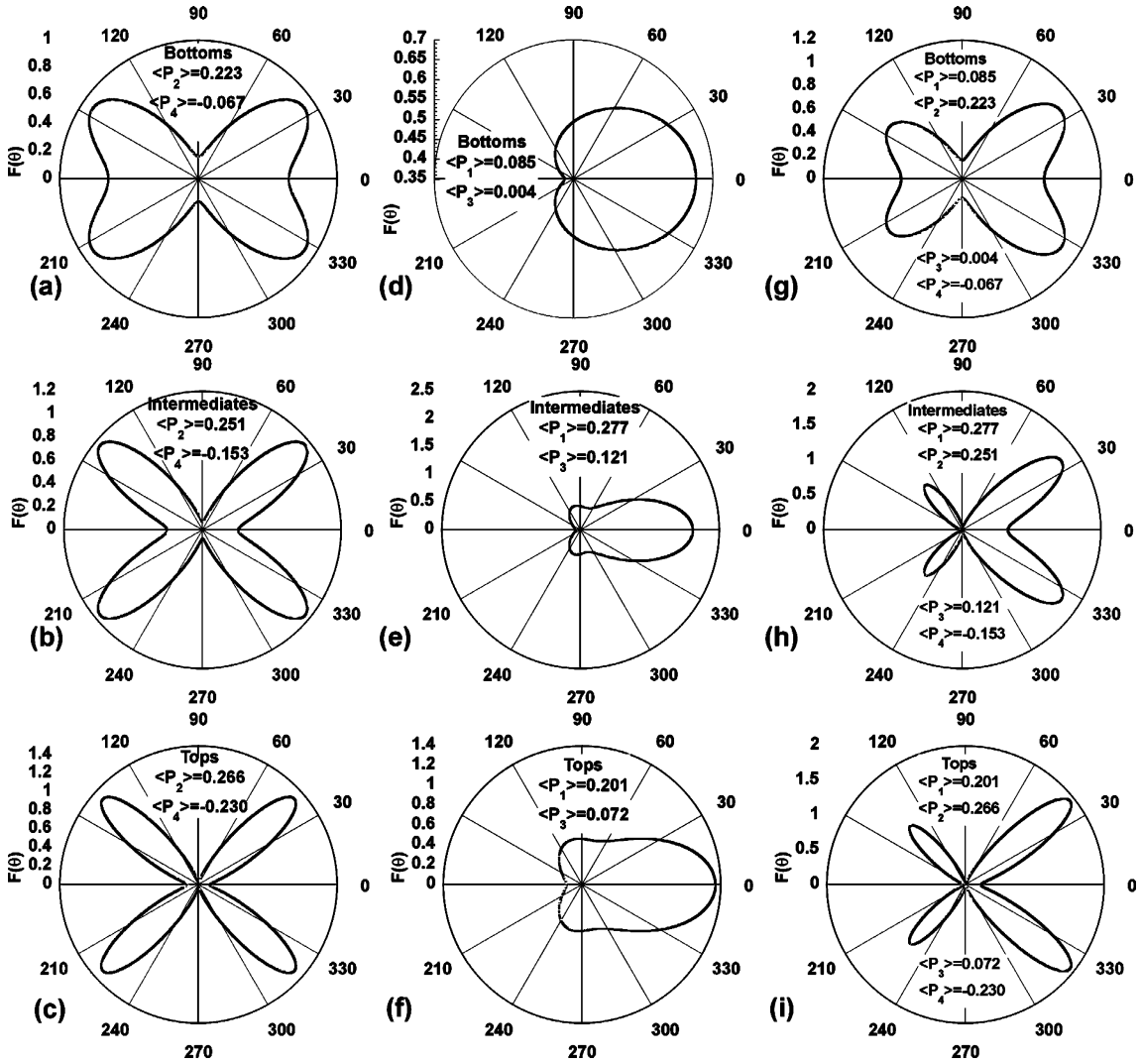

Figure 9. Polar representation of the distribution functions $f(\theta)$ calculated at the bottom, intermediate and top regions of a surface relief grating inscribed in a pDR1M polymer. Distribution functions were calculated using even order parameters, $\langle P_2 \rangle$ and $\langle P_4 \rangle$ (a−c), and odd order parameters $\langle P_1 \rangle$ and $\langle P_3 \rangle$ (d−f). The full distribution functions $f(\langle P_1 \rangle, \langle P_2 \rangle, \langle P_3 \rangle, \langle P_4 \rangle)$ are represented in parts g−i.

existence of increasing force and pressure constraints during the peak relief formation and during the related chromophore diffusion mechanisms. Because of the large force gradients during the isomerization cycles and the angular reorientations, the chromophore orientation distributions appear significantly perturbed by the polymer migration from areas of high field intensity (that correspond to the bottoms of the grating) to area of lower intensity (tops of the grating) (Figure 2).

(ii) For the first time, the $\langle P_1 \rangle$ and $\langle P_3 \rangle$ order parameters are extracted from polarized scanning near-field experiments and they reveal a strong polar ordering of the azobenzene chromophores that have been oriented under an external dc electric field. Similarly to the modulated curve variations of the PP and SP polarized SHG measurements (Figure 7a), the variation curves of $\langle P_1 \rangle$ and $\langle P_3 \rangle$ (Figure 8) exhibit strong modulations. The $\langle P_1 \rangle$ and $\langle P_3 \rangle$ values are larger in the intermediate and top regions, (0.277, 0.121) and (0.201, 0.072), respectively, while they are weak in the bottom regions (0.085, 0.004). Although, these sets of parameters are far from a delta function alignment (for which $\langle P_1 \rangle = \langle P_3 \rangle = 1.0$), our estimated values are significantly larger than those previously determined by Kuzyk et al. for poled thin films (doped PMMA with DR1 azobenzene) without mechanical stress.[48] The distribution functions all display a polar asymmetry along the Z reference direction. As shown in Figure 9e,f, the calculated distribution functions confirm the existence of a strong polar ordering in the top and intermediate regions and less efficient ordering in the bottom of the grating (Figure 9d). Furthermore, it must be pointed out that the variations of $\langle P_1 \rangle$ and $\langle P_3 \rangle$ (Figure 8) exhibit an additional substructure with a half-periodicity, leading to less pronounced wells which are not detected in the Raman images (Figure 4) and the Raman intensity profiles (Figure 5). These wells are surely due to a perturbation in the polar alignment of the chromophores at the half-periods, and they presumably arise from a reduced mobility in the ridges of the grating. This can be assigned to a density increase and an increase in the local glass transition temperature, which reduces the poling efficiency in these areas that become stiffer. Such a modification of the viscoelastic properties of the polymer thin film due to the diffusion of the photosensitive azobenzene chromophores has also been evidenced by tapping mode atomic force microscopy.[49] In that study, the phase image obtained from AFM measurements showed contrast in the viscoelastic properties of the thin film after irradiation. This confirms that the polymer chains have migrated from the stronger optical field regions to the weaker ones and, more importantly, that the weaker field areas were becoming stiffer. In addition, X-ray diffraction measurements performed on thermally erased gratings (the surface topography of which are flattened by annealing above the T_g of the polymer) have demonstrated the presence of density gratings that keep

the memory of the grating periodicity but change their viscoelactic properties.[50]

(iii) Finally, the resulting distribution functions $f(\langle P_1\rangle,\langle P_2\rangle,\langle P_3\rangle,\langle P_4\rangle)$ represent the most probable distributions of the chromophores, as determined from far-field Raman and SHG-NSOM measurements. All orientational distributions show polar asymmetry along the *Z* reference direction, revealing quite efficient poling in the thin film grating in which we can claim that the centrosymmetric arrangement is definitely broken. Overall, the final orientational distributions are very narrow at the intermediate and top positions with their maxima peaked at 35°, indicating a high degree of polar orientation compared to the bottom regions. In addition, the distribution of chromophores purely oriented along the Z direction (0° direction) is significantly higher at the intermediate locations (Figure 9h) compared to the top regions (Figure 9i). This is in agreement with SHG-NSOM images (Figure 4a) and intensity profiles (Figure 7a) where the electrical poling was less efficient in the top areas than in the intermediate locations.

IV. Conclusion

In the present study we have characterized a nonlinear optical diffraction grating that was inscribed in an azobenzene-containing polymer thin film. For the first time, two techniques, confocal Raman microscopy and SHG-NSOM, were used to determine the molecular orientations in different regions of the surface grating. These techniques are complementary since Raman microscopy is sensitive to the average molecular orientations through spectral measurements, whereas the optical contrast relative to the polar orientations is exclusively observed in SHG-NSOM; in addition, the SHG signal is correlated in real time with the sample topography. This combination of far-field confocal microscopy and near-field microscopy is particularly well adapted for the investigation of bulk and surface properties in mesostructured materials.

The Legendre polynomials or order parameter values, were obtained under polarized measurements in Raman for $\langle P_2\rangle$ and $\langle P_4\rangle$, and in SHG-NSOM for $\langle P_1\rangle$ and $\langle P_3\rangle$. Using information entropy theory, the most probable distribution functions were derived in various regions of the grating with submicrometer spatial resolution. They reveal that narrower distribution functions are found in the slopes of the surface relief, while, as shown by SHG-NSOM, a weaker polar ordering is observed at the crest of the ridges of the grating.

These experiments, in conjunction with polarization analysis recordings, have resulted in a better understanding of the optical properties in a nonlinear optical grating, and they emphasize the importance of both Raman and near-field techniques to study nano- and meso-organized objects and surfaces at a molecular level. Integration of Raman measurements with NSOM is a challenging endeavor, but recent work has shown its feasibility, provided that one takes advantage of resonance conditions and/or enhancements of the field from a metallic tip.[51−54] Work in this direction is in progress.

Acknowledgment. The authors are indebted to the CNRS (Chemistry Department) and to Région Aquitaine for financial support for the near-field and micro-Raman equipment. They are also thankful to V. Rodriguez and A. Adamietz for poling assistance and to S. Umapathy for fruitful discussions. The Berkeley group is supported by the Experimental Physical Chemistry Division of the U.S. National Science Foundation.

TABLE 2: Fresnel Factors and Parameters used for the Calculation of the χ_{eff} for ZnSe[55]

	ω	2ω
λ/μm	1.064	0.532
n	2.425	2.630
l_c/nm	17.8	
L_X	0.870	0.836
L_Y	0.361	0.335
L_Z	0.192	0.168
d_{14}/(pm/V)	27	

Appendix. SHG-NSOM Normalization with Respect to a ZnSe Crystal

In the ZnSe crystal used for normalization of the SHG data, which belongs to the T_d symmetry group, only one tensor element is independent, χ_{xyz}, and the effective susceptibilities are

$$\chi_{\text{eff}}^{\text{PP}} = \sin\phi\cos\phi(4L_x(\omega)L_x(2\omega)L_z(\omega)\cos^2\beta\sin\beta - 2L_x^2(\omega)L_z(2\omega)\sin^3\beta)\chi_{xyz}$$

$$\chi_{\text{eff}}^{\text{SP}} = (2\sin\phi\cos\phi L_y^2(\omega)L_z(2\omega)\sin\beta)\chi_{xyz}$$

$$\chi_{\text{eff}}^{\text{45/S}} = (2\sin\phi\cos\phi L_y(\omega)L_y(2\omega)L_z(\omega)\sin\beta - L_y(2\omega)L_z^2(\omega)\cos\beta\sin\beta(\cos^2\phi - \sin^2\phi))\chi_{xyz} \quad \text{(A1)}$$

From these parameters (Table 2) and for an orientation of the crystal of 45°, one gets

$$\chi_{\text{eff}}^{\text{PP}} = -0.0223\chi_{xyz}$$

$$\chi_{\text{eff}}^{\text{SP}} = 0.0191\chi_{xyz}$$

$$\chi_{\text{eff}}^{\text{45/S}} = 0.0202\chi_{xyz} \quad \text{(A2)}$$

The orientation of the crystal is confirmed by the low difference of contrast between the various polarization configurations for the near-field study of the flat surface of ZnSe. Since we know the nonlinear coefficient for SHG at the considered wavelengths, one may write for the reference (ZnSe):

$$\chi_{xyz} = 2d_{14} = 2(27\times10^{-12})\ \text{m/V} = 54\ \text{pm/V at } 1.064\ \mu\text{m}$$

Using eq A2, one gets for ZnSe, in the reflection geometry

$$\chi_{\text{eff}}^{\text{PP}} l_c = -1.94\times10^{-20}\ \text{m}^2\ \text{V}^{-1}$$

$$\chi_{\text{eff}}^{\text{SP}} l_c = 1.836\times10^{-20}\ \text{m}^2\ \text{V}^{-1}$$

$$\chi_{\text{eff}}^{\text{45/S}} l_c = 1.942\times10^{-20}\ \text{m}^2\ \text{V}^{-1} \quad \text{(A3)}$$

Finally, the ratio of the chromophores and reference susceptibilities leads to the final normalized expressions:

$$\left|\frac{\chi_{\text{eff}}^{\text{PP}}(\text{Azo})l_c(\text{Azo})}{\chi_{\text{eff}}^{\text{PP}}(\text{ZnSe})l_c(\text{ZnSe})}\right| = \sqrt{\frac{I^{\text{PP}}(\text{Azo})}{I^{\text{PP}}(\text{ZnSe})}}$$

$$\left|\frac{\chi_{\text{eff}}^{\text{SP}}(\text{Azo})l_c(\text{Azo})}{\chi_{\text{eff}}^{\text{SP}}(\text{ZnSe})l_c(\text{ZnSe})}\right| = \sqrt{\frac{I^{\text{SP}}(\text{Azo})}{I^{\text{SP}}(\text{ZnSe})}} \quad \text{(A4)}$$

References and Notes

(1) Che, Y.; Sugihara, O.; Egami, C.; Fujimura, H.; Kawata, Y.; Okamoto, N.; Tsuchimori, M.; Watanabe, O. *Jpn. J. Appl. Phys.* **1999**, *38*, 6316.

(2) Martin, G.; Toussaere, E.; Soulier, L.; Zyss, J. *Synth. Met.* **2002**, *127*, 49.

(3) Donval, A.; Toussaere, E.; Zyss, J.; Levy-Yurista, G.; Jonsson, E.; Friesem, A. A. *Synth. Met.* **2001**, *124*, 19.

(4) Ju, J. J.; Kim, J.; Do, J. Y.; Kim, M.-s.; Park, S. K.; Park, S.; Lee, M.-H. *Opt. Lett.* **2004**, *29*, 89.

(5) Oki, Y.; Yoshiura, T.; Chisaki, Y.; Maeda, M. *Appl. Opt.* **2002**, *41*, 5030.

(6) Matsui, T.; Ozaki, M.; Yoshino, K.; Kajzar, F. *Jpn. J. Appl. Phys.* **2002**, *41*, 1386.

(7) Rocha, L.; Dumarcher, V.; Denis, C.; Raimond, P.; Fiorini, C.; Nunzi, J.-M. *J. Appl. Phys.* **2001**, *89*, 3067.

(8) Munakata, K.; Harada, K.; Anji, H.; Itoh, M.; Yatagai, T. *Opt. Lett.* **2001**, *26*, 4.

(9) Sugihara, O.; Nakanishi, M.; Fujimura, H.; Egami, C.; Okamoto, N. *Opt. Lett.* **2000**, *25*, 1028.

(10) Apostoluk, A.; Chapron, D.; Gadret, G.; Sahraoui, B.; Nunzi, J.-M.; Fiorini-Debuisschert, C.; Raimond, P. *Opt. Lett.* **2002**, *27*, 2028.

(11) Apostoluk, A.; Nunzi, J.-M.; Fiorini-Debuisschert, C. *Opt. Lett.* *29*, 98.

(12) Blinov, L. M.; Palto, S. P.; Yudin, S. G.; De Santo, M. P.; Cipparone, G.; Mazzulla, A.; Barberi, R. *Appl. Phys. Lett.* **2002**, *80*, 16.

(13) Munakata, K.; Harada, K.; Yoshikawa, N.; Itoh, M.; Umegaki, S.; Yatagai, T. *Opt. Rev.* **1999**, *6*, 518.

(14) Rodriguez, V.; Adamietz, F.; Sanguinet, L.; Buffeteau, T.; Sourisseau, C. *J. Phys. Chem. B* **2003**, *107*, 9736.

(15) Schaller, R. D.; Saykally, R. J.; Shen, Y. R.; Lagugné-Labarthet, F. *Opt. Lett.* **2003**, *28*, 1296.

(16) Delaire, J.; Nakatani, K. *Chem. Rev.* **2000**, *100*, 1817.

(17) Rodriguez, V.; Sourisseau, C. *J. Opt. Soc. Am.* **2002**, *19*, 2650.

(18) Dunn, R. C. *Chem. Rev.* **1999**, *99*, 2891.

(19) Kinoshita, Y.; Park, B.; Takezoe, H.; Niori, T.; Watanabe, J. *Langmuir* **1998**, *14*, 6256.

(20) Wang, J.; Paszti, Z.; Even, M. A.; Chen, Z. *J. Am. Chem. Soc.* **2002**, *124*, 7016.

(21) Kim, D.; Oh-e, M.; Shen, Y. R. *Macromolecules* **2001**, *24*, 9125.

(22) Lagugné-Labarthet, F.; Buffeteau, T.; Sourisseau, C. *J. Phys. Chem. B* **1998**, *102*, 5754.

(23) Lagugné-Labarthet, F.; Bruneel, J. L.; Buffeteau, T.; Sourisseau, C.; Huber, M. R.; Zilker, S. J.; Bieringer, T. *Phys. Chem. Chem. Phys.* **2000**, *2*, 5154.

(24) Lagugné-Labarthet, F.; Bruneel, J. L.; Rodriguez, V.; Sourisseau, C. *J. Phys. Chem. B* **2004**, *108*, 1267.

(25) Lagugné-Labarthet, F.; Bruneel, J. L.; Buffeteau, T.; Sourisseau, C. *J. Chem. Phys. B* **2004**, *108*, 6949.

(26) Lagugné-Labarthet, F.; Bruneel, J. L.; Sourisseau, C.; Huber, M. R.; Borger, V.; Menzel, H. *J. Raman Spectrosc.* **2001**, *32*, 665.

(27) Lagugné-Labarthet, F.; Buffeteau, T.; Sourisseau, C. *J. Appl. Phys. B* **2002**, *74*, 129.

(28) Xie, X. S.; Dunn, R. C. *Science* **1994**, *265*, 361.

(29) Trautman, J. K.; Macklin, J. J. *J. Chem. Phys. B* **1996**, *205*, 221.

(30) Schaller, R. D.; Roth, C.; Raulet, D. H.; Saykally, R. J. *J. Chem. Phys. B* **2000**, *104*, 5217.

(31) Schaller, R. D.; Johnson, J. C.; Wilson, K. R.; Lee, L. F.; Haber, L. H.; Saykally, R. J. *J. Phys. Chem. B* **2002**, *106*, 5143.

(32) Schaller, R. D.; Lee, L. F.; Johnson, J. C.; Haber, L. H.; Saykally, R. J. *J. Phys. Chem. B* **2002**, *106*, 9496.

(33) Schaller, R. D.; Saykally, R. J.; Shen, Y. R.; Lagugné-Labarthet, F. *Proc. SPIE* **2003**, *4991*, 305.

(34) Lagugné-Labarthet, F.; Buffeteau, T.; Sourisseau, C. *J. Phys. Chem. B* **1999**, *103*, 6690.

(35) Kim, K. H.; Miyachi, K.; Ishikawa, K.; Takezoe, H.; Fukuda, A. *Jpn. J. Appl. Phys.* **1994**, *33*, 5850.

(36) Lagugné-Labarthet, F.; Buffeteau, T.; Sourisseau, C. *Appl. Spectrosc.* **2000**, *54*, 699.

(37) Yoo, J.-G.; Hoshi, H.; Sakai, T.; Park, B.; Ishikawa, K.; Takezoe, H.; Lee, Y. S. *J. Appl. Phys.* **1998**, *84*, 4079.

(38) Yoo, J.-G.; Park, B.; Sakai, T.; Kinoshita, Y.; Hoshi, H.; Ishikawa, K.; Takezoe, H. *Jpn. J. Appl. Phys.* **1998**, *37*, 4124.

(39) Sakai, T.; Park, B.; Yoo, J.-G.; Hoshi, H.; Ishikawa, K.; Takezoe, H. *Mol. Cryst. Liq. Cryst.* **1998**, *322*, 49.

(40) Berne, B. J.; Pechukas, P.; Haro, G. D. *J. Chem. Phys.* **1968**, *49*, 3125.

(41) Kinosita, K. J.; Kawato, S.; Ikegami, A. *Biophys. J.* **1977**, *20*, 289.

(42) Pottel, H.; W.; van der Meer, B. W.; Ameloot, M. *Chem. Phys.* **1986**, *102*, 37.

(43) Park, B.; Yoo, J.-G.; Sakai, T.; Hoshi, H.; Ishikawa, K.; Takezoe, H. *Phys. Rev. E* **1998**, *58*, 4624.

(44) Sourisseau, C.; Maraval, P. *Appl. Spectrosc.* **2003**, *57*, 1324.

(45) Feller, M. B.; Chen, W.; Shen, Y. R. *Phys. Rev. A* **1991**, *43*, 6779.

(46) Wagner, H. P.; Kühnelt, M.; Langbein, W.; Hyam, J. M. *Phys. Rev. B* **1998**, *58*, 10494.

(47) Kaatz, N.; Shelton, D. P. *J. Chem. Phys. B* **1996**, *105*, 3918.

(48) Kuzyk, M. G.; Singer, K. D.; Zahn, H. E.; King, L. A. *J. Opt. Soc. Am.* **1989**, *6*, 742.

(49) Ikawa, T.; Mitsuoka, T.; Hasegawa, M.; Tsuchimori, M.; Watanabe, O.; Kawata, Y.; Egami, C.; Sugihara, O.; Okamoto, N. *J. Phys. Chem. B* **2000**, *104*, 9055.

(50) Geue, T. M.; Saphiannikova, M. G.; Henneberg, O.; Pietsch, U.; Rochon, P. L.; Natansohn, A. L. *Phys. Rev. E.* **2002**, *65*, 052801.

(51) Hartschuh, A.; Sanchez, E.; Xie, X. S.; Novotny, L. *Phys. Rev. Lett.* **2003**, *90*, 0955031.

(52) Hallen, H. D.; Jahncke, C. L. *J. Raman Spectrosc.* **2003**, *34*, 655.

(53) Bouhelier, A.; Beversluis, M.; Hartschuh, A.; Novotny, L. *Phys. Rev. Lett.* **2003**, *90*, 13903.

(54) Hartschuh, A.; Beversluis, M. R.; Bouhelier, A.; Novotny, L. *Philos. Trans. R. Soc. London A* 2004.

(55) Adachi, S.; Taguchi, T. *Phys. Rev. B* **1991**, *43*, 9569.